



OPEN ACCESS

EDITED BY

Pulkit Khandelwal,
University of Pennsylvania, United States

REVIEWED BY

Sethu K. Boopathy Jegathambal,
McGill University, Canada
Chiara Mauri,
Massachusetts General Hospital and Harvard
Medical School, United States

*CORRESPONDENCE

Serena J. Counsell
✉ Serena.Counsell@kcl.ac.uk

RECEIVED 27 November 2024

ACCEPTED 10 April 2025

PUBLISHED 09 May 2025

CITATION

Gal-Er B, Brackenier Y, Bonthron AF, Casella C, Price A, Arulkumaran S, Chew ATM, Nosarti C, Cleri M, Cio PD, Egloff A, Rutherford MA, O'Muircheartaigh J, Tomi-Tricot R, Malik S, Cordero-Grande L, Hajnal JV and Counsell SJ (2025) Verifying the concordance between motion corrected and conventional MPRAGE for pediatric morphometric analysis. *Front. Neurosci.* 19:1534924. doi: 10.3389/fnins.2025.1534924

COPYRIGHT

© 2025 Gal-Er, Brackenier, Bonthron, Casella, Price, Arulkumaran, Chew, Nosarti, Cleri, Cio, Egloff, Rutherford, O'Muircheartaigh, Tomi-Tricot, Malik, Cordero-Grande, Hajnal and Counsell. This is an open-access article distributed under the terms of the [Creative Commons Attribution License \(CC BY\)](https://creativecommons.org/licenses/by/4.0/). The use, distribution or reproduction in other forums is permitted, provided the original author(s) and the copyright owner(s) are credited and that the original publication in this journal is cited, in accordance with accepted academic practice. No use, distribution or reproduction is permitted which does not comply with these terms.

Verifying the concordance between motion corrected and conventional MPRAGE for pediatric morphometric analysis

Barat Gal-Er¹, Yannick Brackenier^{1,2}, Alexandra F. Bonthron¹, Chiara Casella^{1,3}, Anthony Price^{1,4}, Sophie Arulkumaran¹, Andrew T. M. Chew¹, Chiara Nosarti¹, Michela Cleri², Pierluigi Di Cio², Alexia Egloff¹, Mary A. Rutherford¹, Jonathan O'Muircheartaigh^{1,3}, Raphael Tomi-Tricot^{1,2,5}, Shaihan Malik^{1,2}, Lucilio Cordero-Grande^{1,2,6}, Joseph V. Hajnal^{1,2} and Serena J. Counsell^{1*}

¹Centre for the Developing Brain, Research Department of Early Life Imaging, School of Biomedical Engineering and Imaging Sciences, King's College London, London, United Kingdom, ²Research Department of Imaging Physics and Engineering, School of Biomedical Engineering and Imaging Sciences, King's College London, London, United Kingdom, ³Department of Forensic and Neurodevelopmental Sciences, Institute of Psychiatry, Psychology and Neuroscience, King's College London, London, United Kingdom, ⁴Guy's and St Thomas' NHS Foundation Trust, London, United Kingdom, ⁵MR Research Collaborations, Siemens Healthcare Limited, Camberley, United Kingdom, ⁶Biomedical Image Technologies, ETSI Telecomunicación, Universidad Politécnica de Madrid and CIBER-BNN, ISCIII, Madrid, Spain

Purpose: This study aimed to validate a retrospective motion correction technique, Distributed and Incoherent Sample Orders for Reconstruction Deblurring using Encoding Redundancy (DISORDER), for pediatric brain morphometry.

Methods: Two T1-weighted MPRAGE 3D datasets were acquired at 3 T in thirty-seven children aged 7–8 years: one with conventional linear phase encoding and one using DISORDER. MPRAGE images were scored as motion-free or motion-corrupt. Cortical morphometry and regional brain volumes were measured with FreeSurfer, subcortical grey matter (GM) with FSL-FIRST, and hippocampi with HippUnfold. Intraclass correlation coefficient (ICC) was used to determine agreement. Mann–Whitney *U* was used to test the difference between measures obtained using DISORDER and (i) motion-free and (ii) motion-corrupt conventional MPRAGE data.

Results: ICC measures between conventional MPRAGE and DISORDER data were good/excellent for most subcortical GM (motion-free, 0.75–0.96; motion-corrupt, 0.62–0.98) and regional brain volumes (motion-free 0.47–0.99; motion-corrupt, 0.54–0.99), except for the amygdala and nucleus accumbens (motion-free, 0.38–0.65; motion-corrupt, 0.1–0.42). These values were less consistent for motion-corrupt conventional MPRAGE data for hippocampal volumes (motion-free 0.65–0.99; motion-corrupt, 0.11–0.91) and cortical measures (motion-free 0.76–0.98; motion-corrupt, 0.09–0.74). Mann–Whitney *U* showed percentage differences in measures obtained with motion-corrupt conventional MPRAGE compared to DISORDER data were significantly greater than in those obtained using motion-free conventional MPRAGE data in 22/58 structures.

Conclusion: In the absence of motion, morphometric measures obtained using DISORDER are largely consistent with those from conventional MPRAGE data, whereas improved reliability is obtained by DISORDER for motion-degraded scans. This study validates the use of DISORDER for brain morphometric studies in children.

KEYWORDS

brain, MRI, pediatric, motion correction, morphometry

Introduction

Structural magnetic resonance imaging (MRI) provides detailed information about brain morphometry. However, obtaining high-quality MR images in children can be challenging. In a clinical setting, good quality MRI data are essential for accurate radiological assessment and in research, high quality imaging data are required to assess morphometry. Head motion, in particular, is a common cause of image degradation in pediatric research settings and motion-induced artifacts can significantly influence estimates of brain metrics derived from MRI (Reuter et al., 2015; Gilmore et al., 2021; Ai et al., 2021).

Multiple strategies are available for correcting intra-scan motion, including prospective and retrospective methods. Prospective methods track data describing the head pose, which is used to update the acquisition in real-time to ensure the field-of-view (FOV) remains aligned with the moving head (Maclaren et al., 2013). These approaches are applicable across a wide range of sequences and scanners, however, they may require additional hardware and scanner modifications (Maclaren et al., 2013). Retrospective motion correction techniques first collect k -space data and then correct for the effects of motion following acquisition, during the reconstruction stage. In a pediatric cohort, a retrospective technique improved T1-weighted image quality and automated segmentation of cortical and subcortical structures compared to a prospective motion correction technique (Kecskemeti and Alexander, 2020). Retrospective motion correction techniques include Distributed and Incoherent Sample Orders for Reconstruction Deblurring by using Encoding Redundancy (DISORDER), a sampling re-ordering scheme in the phase encoding plane (Cordero-Grande et al., 2020; Cordero-Grande et al., 2016) which has been shown to improve image quality in a pediatric cohort (Vecchiato et al., 2021). However, brain morphometric measures obtained from DISORDER data have not been evaluated.

In addition to the sequence used to acquire the images, the choice of software for automated segmentation of brain structures needs to be considered. Several software packages are available for MRI structural analyses, including FreeSurfer [9], and FSL-FIRST (Patenaude et al., 2011). These segmentation tools have been used in cortical and subcortical GM morphometric analyses in pediatric studies (Biffen et al., 2020; Lidauer et al., 2022; Mayer et al., 2016; Pulli et al., 2022; Sandman et al., 2014; Schoemaker et al., 2016; Thompson-Lake et al., 2022). Previous work has suggested that FreeSurfer performs best in cortical analyses (Pulli et al., 2022), and FSL-FIRST is closer to manual segmentation in subcortical grey matter (GM) analyses in pediatric populations (Lidauer et al., 2022). HippUnfold is a recently developed hippocampal-specific segmentation approach (DeKraker et al., 2022) and has been used previously to delineate hippocampal subfields in a pediatric population (Ripart et al., 2023).

The aim of this study was to evaluate the use of DISORDER (Cordero-Grande et al., 2020) in children aged 7–8 years.

Conventional linear phase encoding and DISORDER Magnetization Prepared Rapid Gradient-Echo (MPRAGE) acquisitions were acquired. Brain morphometric measures were obtained using FreeSurfer (Fischl et al., 2002), FSL-FIRST (Patenaude et al., 2011) and HippUnfold (DeKraker et al., 2022) and these measures were compared between the two MPRAGE acquisitions.

Materials and methods

Participants

Data for this study were acquired as part of the ICONIC (Impact of Congenital Heart Disease on Neurodevelopment in Childhood) study between August 2022 and August 2023. Research ethics committee approval was granted (Ref: 22/WA/0014). Informed, written parental consent was obtained and written assent was obtained from participants.

Magnetic resonance imaging acquisition

MRI was performed on a 3 T scanner (MAGNETOM Vida, Siemens Healthcare, Erlangen, Germany) located at St Thomas' Hospital (London, UK). The children were asked to stay still during scanning while watching a movie of their choice. Two T1 weighted MPRAGE 3D image datasets were acquired in the sagittal plane; one with conventional linear phase encoding (referred to as conventional MPRAGE) (TR = 2,200 ms, TE = 2.46 ms, flip angle = 8°, FOV = 204 × 224 × 176, voxel size = 1.1 × 1.07 × 1.07 mm³, acceleration factor = 2, acquisition time = 4.15 min) and one using the DISORDER scheme (TR = 2,200 ms, TE = 2.45 ms, flip angle = 8°, FOV = 210 × 224 × 176, voxel size = 1.1 × 1.07 × 1.07 mm³, no acceleration, acquisition time = 7.39 min). T2-weighted turbo spin echo, diffusion-weighted imaging, fluid attenuated inversion recovery imaging, and resting-state functional MRI were also acquired but not analysed as part of this study.

Motion correction

Rigid-body motion correction ability is sensitive to the k -space encoding order (Cordero-Grande et al., 2020; Cordero-Grande et al., 2016). Combined with the aligned sensitivity encoding (SENSE) framework, which achieves intrascan motion estimation and correction by dividing k -space samples and accounting for different motion states in each temporal segment (Cordero-Grande et al., 2016), DISORDER aims to improve motion tolerance of volumetric structural brain MRI by ensuring that the acquisition of each shot of k -space contains a series of samples distributed incoherently

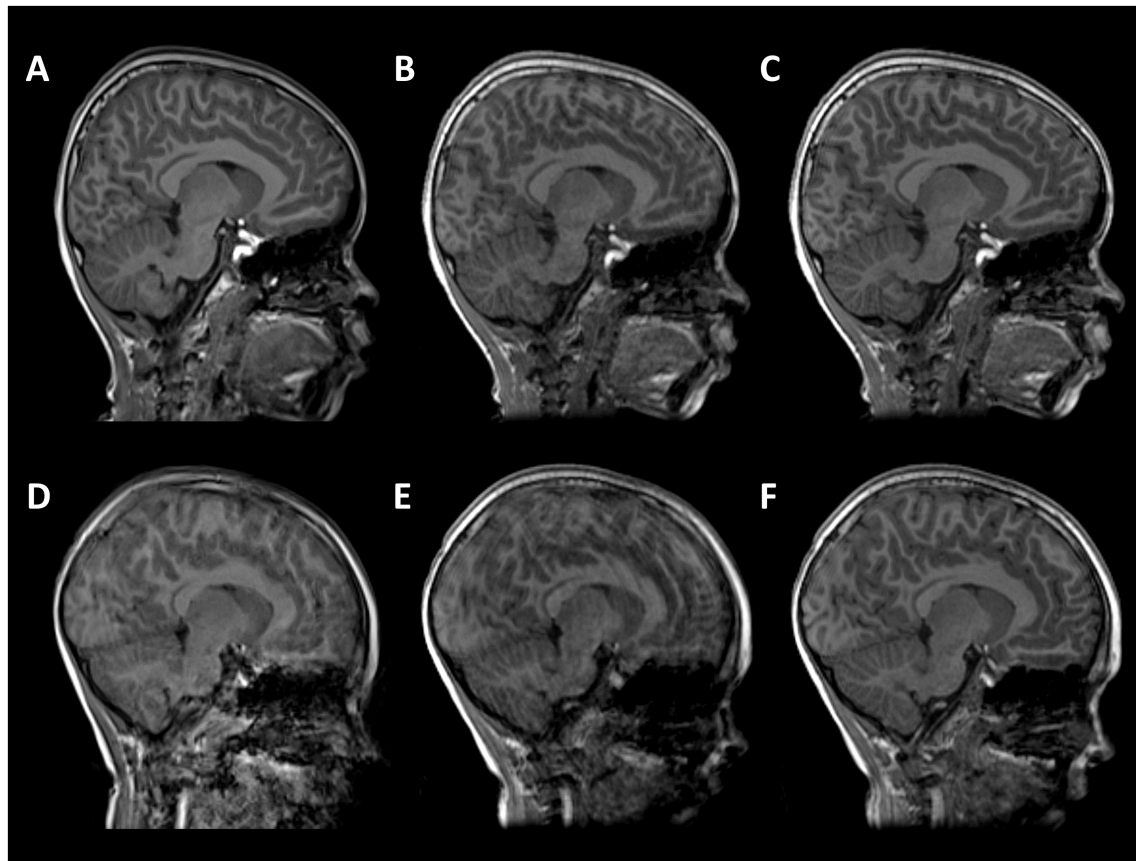


FIGURE 1

T1-weighted MPRAGE images from two subjects. (A–C) male, 7 years 11 months with good quality conventional MPRAGE data; (D–F) male, 7 years 9 months with motion-corrupt conventional MPRAGE data. (A,D) conventional MPRAGE (B,E) DISORDER before motion correction and (C,F) DISORDER after motion correction.

throughout k -space (Cordero-Grande et al., 2020). Since every shot contains samples distributed in k -space, low and high resolution information is available for motion estimation and chances are reduced for large, uncovered k -space areas after a given rotation compensation is applied in reconstruction (Cordero-Grande et al., 2020). These significantly increase the ability to estimate head pose and obtain high-quality motion corrected reconstructions in the presence of rigid motion (Cordero-Grande et al., 2020).

For reconstruction, the motion parameters and the image are jointly estimated. Starting from a reconstruction assuming no motion, a first approximation of the motion parameters for each k -space shot is estimated. Then a new volume is reconstructed with the motion parameters, and the method alternates between motion estimation and reconstruction until convergence (Cordero-Grande et al., 2020; Cordero-Grande et al., 2016). DISORDER reconstruction was performed using MATLAB R2018b (MathWorks, Inc., Natick, Massachusetts), and implemented based on its open-source implementation.¹ Figure 1 shows MPRAGE data acquisitions from two subjects: (A, D) conventional MPRAGE, (B, E) uncorrected and (C, F) motion corrected MPRAGE acquired with the DISORDER scheme.

Image quality evaluation

Image quality was visually inspected by a pediatric neuroradiologist with more than 10 years of experience and an experienced image analyst. Sagittal, coronal and axial views of the MPRAGE data were presented to the raters independently in a randomized and blinded fashion and the images were allocated a binary score: either (i) no evidence of motion (referred to as motion-free) or (ii) evidence of motion (referred to as motion-corrupt).

Image preprocessing

After motion correction, the MPRAGE data underwent intensity normalization using ANTs with parameters set to default (Tustison et al., 2010). Removal of Gibbs ringing artefacts was performed using a 3D extension to the unringing method proposed by Kellner and colleagues (*mrdeGibbs3D*)² with parameters set to default (Bautista et al., 2021; Kellner et al., 2016). Supplementary Figure 1 shows an example of an MPRAGE

¹ Available at <https://github.com/mriphysics/DISORDER>

² <https://github.com/jdtournier/mrdegibbs3D>

dataset before and after Gibbs unringing. Following bias field correction and unringing, images were preprocessed using the Human Connectome Project (HCP) minimal preprocessing pipeline (Glasser et al., 2013).

MPRAGE data were aligned to MNI space using rigid registration (Glasser et al., 2013). After this alignment, an initial brain extraction was performed using linear and non-linear registration of the image to the MNI template (Glasser et al., 2013). The MPRAGE data were skull-stripped using SynthStrip, a deep learning-based brain extraction tool (Hoopes et al., 2022). Using an optimized version of FreeSurfer's recon-all pipeline (FreeSurfer v7.3.2),³ (Glasser et al., 2013; Dale et al., 1999; Fischl et al., 1999), brain tissue was segmented into white matter (WM), grey matter (GM) and cerebrospinal fluid (CSF), and white and pial cortical surfaces were reconstructed (Dale et al., 1999).

Metrics of interest

Subcortical GM volumes (thalamus, caudate nucleus, putamen, globus pallidus, amygdala, nucleus accumbens and brainstem) were segmented and volumes extracted using FSL-FIRST v6.0.5.2 (Patenaude et al., 2011).

Total hippocampal and hippocampal subfield volumes were segmented and volumes extracted using HippUnfold (DeKraker et al., 2022). HippUnfold uses a U-Net neural network architecture to segment hippocampal GM and structures surrounding the hippocampus. Volumetric subfields were generated by filling the voxels between inner and outer surfaces with the corresponding subfield labels (DeKraker et al., 2022). Subfield segmentations include the cornu ammonis (CA1, CA2, CA3, CA4), subiculum, dentate gyrus (DG) and the stratum radiatum lacunosum and moleculare (SRLM) (Figure 2).

Volumes and surfaces generated using FreeSurfer were converted to standard formats used by Connectome Workbench, and a volume segmentation of the cortical ribbon was generated (Glasser et al., 2013). WM, ventral diencephalon, corpus callosum (anterior, mid-anterior, central, mid-posterior, posterior), lateral ventricles, third ventricle, fourth ventricle, cerebellar cortex, cerebellar WM and total cerebellum (cerebellar cortex + cerebellar WM) volumes were extracted using FreeSurfer.

Cortical GM measures (cortical surface area (SA), cortical GM volume, cortical thickness (CT), mean curvature, cortical gyrification) were also extracted using FreeSurfer. Cortical parcellations were computed based on the Desikan-Killiany atlas (Desikan et al., 2006). Cortical thickness was calculated as the average distance between the GM/WM boundary and the pial surface at each vertex within each region of interest (ROI) (Dale et al., 1999). The surface area was calculated on the pial surface as the sum of the areas of each tessellation falling within a given ROI (Dale et al., 1999). Mean curvature is calculated as the average of the principal curvatures, which are derived from the inverse radius of circles at each point on the pial-white matter border. Global measures of CT, surface area, mean curvature and GM volume were calculated as averages or sum totals of these ROIs. To measure cortical gyrification, a local gyrification index value (IGI) was

computed for every vertex on the pial surface of the brain (Schaer et al., 2008; Schaer et al., 2012). The IGI at each vertex of the reconstructed cortical surface was measured as the ratio between the inner buried contour of the cortex and the smoothed outer perimeter, resulting in individual gyrification maps (Schaer et al., 2008; Schaer et al., 2012). The average value of all the individual vertex IGI values was used to calculate the mean IGI for each hemisphere (Schaer et al., 2008; Schaer et al., 2012).

Visual inspection of segmentations

Prior to statistical analysis, all segmentations were manually inspected using Freeview to ensure the accuracy of the cortical ribbon and tissue segmentation. Manual corrections were performed if delineation of the pial surface and WM boundary was poor, with defects spanning multiple slices. Edits were made according to instructions provided by FreeSurfer developers.⁴

Statistical analysis

Statistical analyses were performed and graphs were generated using R v4.2.2⁵ and R-Studio.⁶ Data were assessed for normality using Shapiro–Wilk tests, skewness, and kurtosis values. Descriptive statistics are shown as mean and standard deviation for normally distributed data and median and range for variables with a skewed distribution. False discovery rate (FDR) was used to correct for multiple comparisons and pFDR < 0.05 was considered significant (Benjamini and Hochberg, 1995).

Intraclass correlation coefficients

Intraclass correlation coefficient (ICC) is an established measure of agreement between raters/measures. Here we calculated ICC as a measure of agreement for all morphological measures extracted from both MPRAGE acquisitions. The ICC is calculated as the proportion of overall variance that is explained by between-subject variance. ICC values greater than 0.90 indicate excellent reliability, values between 0.75 and 0.9 indicate good reliability, values between 0.5 and 0.75 indicate moderate reliability and values less than 0.5 are indicative of poor reliability (Koo and Li, 2016).

Percentage difference between brain morphometric measures

In order to assess the difference between morphometric measures obtained using DISORDER and (i) motion-free and (ii) motion-corrupt conventional MPRAGE images, the percentage difference between measures was computed using the formula: Percentage difference = [(DISORDER – conventional MPRAGE)/conventional

³ <https://surfer.nmr.mgh.harvard.edu/>

⁴ <https://surfer.nmr.mgh.harvard.edu/fswiki/FsTutorial/TroubleshootingData>

⁵ <https://www.r-project.org/>

⁶ <https://rstudio.com/>

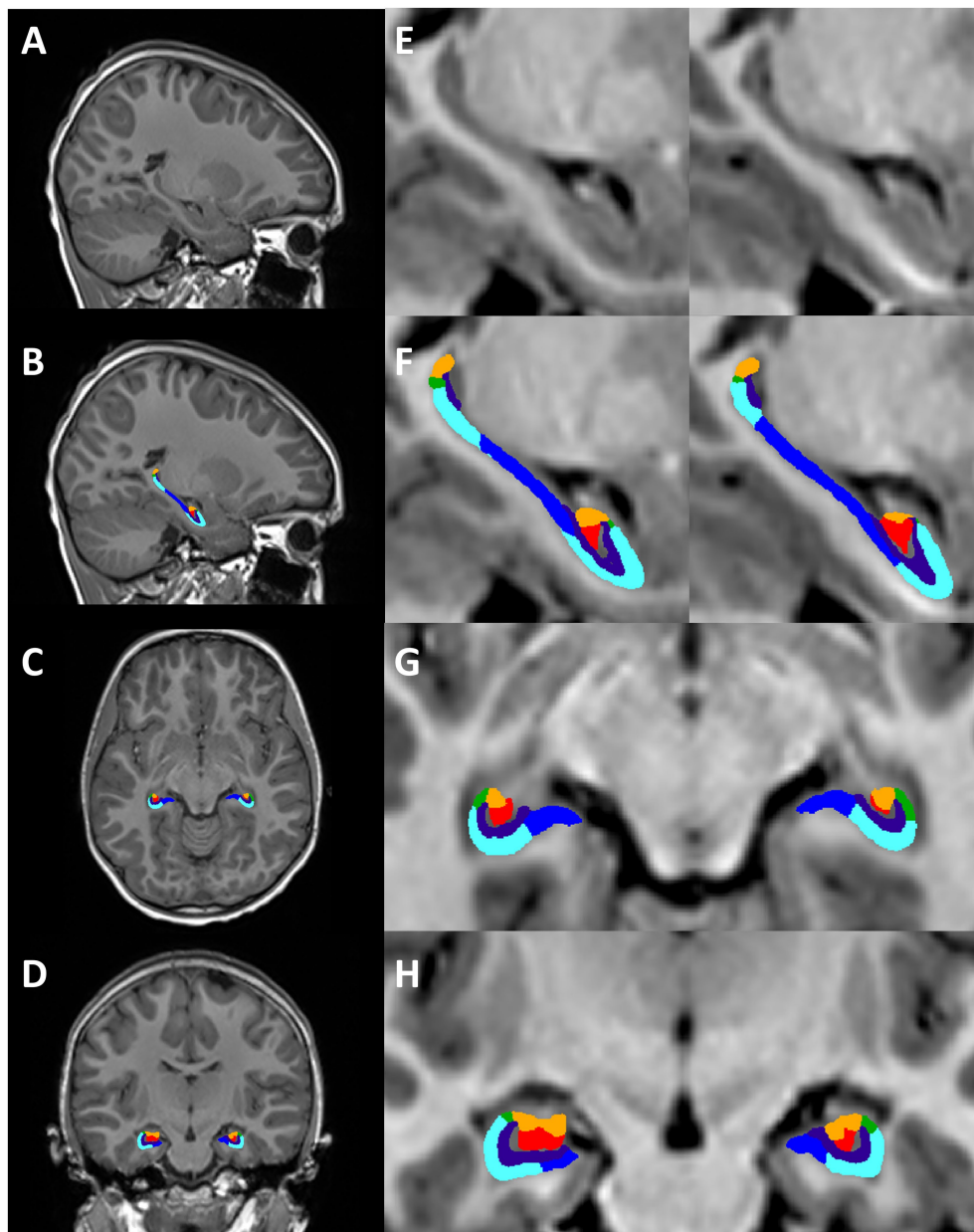


FIGURE 2

Hippocampal segmentation from one representative subject (female, 7 years 11 months). Motion-free conventional MPRAGE (A,E) and segmentation of the hippocampus using HippUnfold in the sagittal (B,F), axial (C,G), and coronal planes (D,H). Hippocampal subfields; subiculum (dark blue), CA1 (light blue), CA2 (green), CA3 (orange), CA4 (red), SRLM (purple).

MPRAGE] * 100 (Schoemaker et al., 2016). Negative values indicate an underestimation of measures obtained with DISORDER compared to the conventional MPRAGE, while positive values indicate an overestimation of measures obtained with DISORDER relative to conventional MPRAGE data. Mann-Whitney U was used to test the effect of motion on the percentage difference.

Sensitivity analyses

In order to assess whether participants with CHD biased the results, ICC and percentage difference analyses were repeated after removing individuals with CHD.

Hemispheric differences in brain morphometric measures

To assess hemispheric differences in morphometric measures, the percentage difference between left and right measures was computed using the formula: Percentage difference = $[(\text{Left} - \text{Right}) / (\text{Left} + \text{Right})] * 100$. Negative values indicate that the right morphometric measure is larger than the left, while positive values indicate that the left morphometric measure is larger than the right. Mann-Whitney U was used to test whether there were significant differences between the hemispheric percentage difference morphometric measures obtained using DISORDER and (i) motion-free and (ii) motion-corrupt conventional MPRAGE data.

Results

Participants

Sixty children were enrolled in the ICONIC study between August 2022 and August 2023, including 12 children with congenital heart disease (CHD) and 48 healthy controls. Twenty-three children were excluded from the analysis; conventional MPRAGE data not acquired ($n = 20$), MPRAGE with DISORDER data not acquired ($n = 3$). The final analysis included 37 children who underwent MR imaging at a median (range) age of 7.75 (7.5–8.33) years (Table 1); 20 children with motion-free conventional MPRAGE data and 17 children with motion-corrupt conventional MPRAGE data.

The two raters were in complete agreement regarding image motion scores. Of the 17 children with motion-corrupt conventional MPRAGE data, 14 children had motion-free DISORDER data and 3 children had DISORDER data with minimal motion following reconstruction. All 20 children with motion-free conventional MPRAGE data had motion-free DISORDER data following reconstruction. FreeSurfer's reconstruction and segmentation failed in 1 child with motion-corrupt conventional MPRAGE data however, FSL-FIRST and HippUnfold were able to segment subcortical GM structures and hippocampal subfields, respectively, in this participant.

Thirteen out of the 74 MPRAGE datasets required manual editing (Supplementary Table 1). Example conventional MPRAGE and DISORDER images with cortical segmentation overlays are shown in Figure 3 for a subject with motion-free conventional MPRAGE and a subject with motion-corrupt conventional MPRAGE data (Figure 3).

Results of analyses comparing conventional MPRAGE and DISORDER data

Intraclass correlation coefficients

Subcortical grey matter volumes

ICC measures between motion-free conventional MPRAGE data and DISORDER data were excellent for the bilateral thalamus, bilateral caudate nucleus and brainstem; good for the bilateral putamen and globus pallidus; moderate for the right amygdala and left nucleus accumbens; and poor for the left amygdala and right nucleus accumbens (Table 2).

ICC measures between motion-corrupt conventional MPRAGE and DISORDER data were excellent for the thalamus bilaterally; good for the bilateral putamen, bilateral globus pallidus, left caudate nucleus and brainstem; moderate for the

TABLE 1 Demographics of the study population.

Demographics	Motion-free conventional MPRAGE (N = 20)	Motion-corrupt conventional MPRAGE (N = 17)	Total (N = 37)
Median age at scan [range], (years)	7.75 [7.5–8.17]	7.83 [7.58–8.33]	7.75 [7.5–8.33]
Male, no (%)	10 (50)	10 (59)	20 (54)
CHD, no (%)	4 (20)	2 (12)	6 (16)

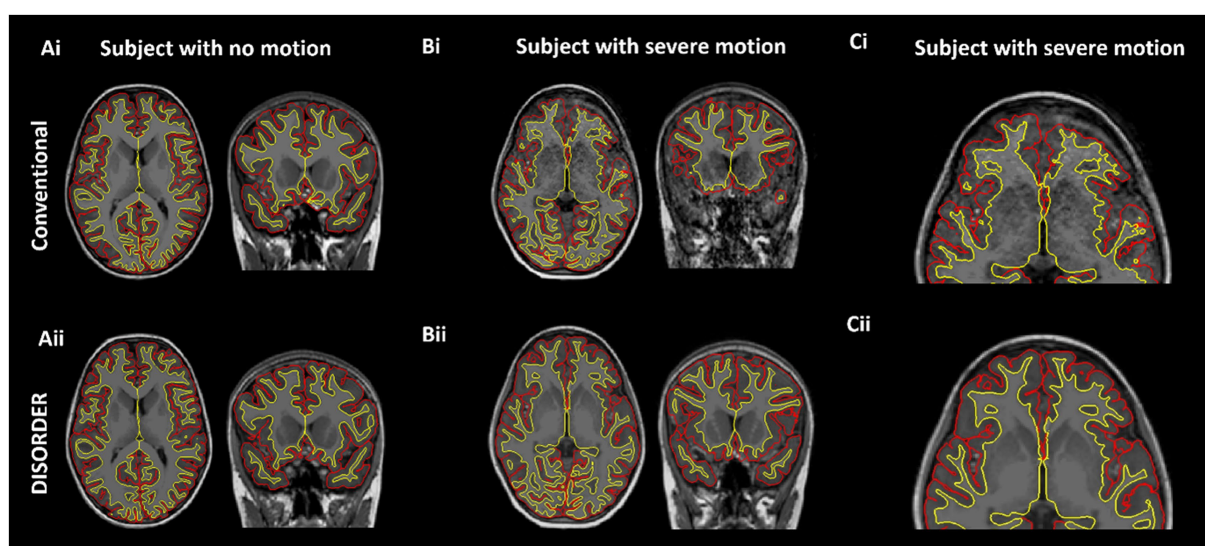


FIGURE 3

Cortical segmentations. The top row shows conventional MPRAGE acquisitions and the bottom row shows the DISORDER MPRAGE acquisition. (Ai,Aii) Female, 7 years 8 months no head motion. (Bi–Cii) Female, 8 years with severe head motion. (Ci) Motion corrupt conventional MPRAGE data created incorrect pial (red) and white matter (yellow) boundaries while DISORDER data (Cii) resulted in accurate cortical segmentations.

TABLE 2 ICC and percentage differences between subcortical grey matter volumes obtained with conventional MPRAGE and DISORDER data.

Region	Motion-free conventional MPRAGE				Motion-corrupt conventional MPRAGE			
	Conventional MPRAGE ($\times 10^3$ mm ³)	DISORDER MPRAGE ($\times 10^3$ mm ³)	ICC	%D	Conventional MPRAGE ($\times 10^3$ mm ³)	DISORDER MPRAGE ($\times 10^3$ mm ³)	ICC	%D
Left Thalamus	8.14 (6.88–9.65)	7.72 (6.51–9.53)	0.96	–1.8 (–6.2–4.1)	8.12 (6.90–9.63)	7.84 (6.90–9.44)	0.98	–1.4 (–6.2–2.7)
Right Thalamus	7.75 (6.57–9.22)	7.56 (6.22–8.98)	0.96	–2.3 (–6.6–1.7)	7.84 (6.34–9.29)	7.5 (6.43–9.17)	0.97	–2.4 (–6.3–2.1)
Left Caudate	3.76 (3.29–4.84)	3.63 (3.17–4.52)	0.93	–2.4 (–11.4–7.0)	3.48 (2.99–4.67)	3.48 (2.98–4.77)	0.75	3.2 (–12.5–16.1)
Right Caudate	4.06 (2.99–5.08)	3.84 (2.71–4.88)	0.93	–3.2 (–16.0–6.5)	3.48 (2.99–4.67)	3.61 (3.17–4.63)	0.62	4.6 (–14.7–13.8)
Left Putamen	5.06 (4.05–5.86)	4.64 (3.78–5.18)	0.75	–8.1 (–16– –2.3)	4.47 (3.47–6.32)	4.32 (3.58–5.77)	0.88	–2.3 (–11.0–20.1)
Right Putamen	4.89 (4.11–5.84)	4.53 (3.87–5.20)	0.76	–7.8 (–15– –3.5)	4.30 (3.47–6.19)	4.10 (3.47–5.40)	0.85	–5.9 (–11.8–10.5)
Left GP	1.67 (1.37–1.84)	1.59 (1.27–1.72)	0.82	–2.3 (–7.7–4.6)	1.61 (1.38–1.86)	1.58 (1.25–1.76)	0.77	–2.5 (–10.6–8.2)
Right GP	1.61 (1.35–1.83)	1.56 (1.28–1.80)	0.89	–6.3 (–10.8–2.3)	1.53 (1.29–1.91)	1.52 (1.32–1.76)	0.88	–0.9 (–7.5–8.1)
Left Amygdala	1.20 (0.99–1.54)	1.38 (1.11–1.70)	0.38	10.0 (–6.1–43.3)	1.17 (0.69–1.54)	1.43 (0.93–1.69)	0.26	22.2 (–2.4–97.9)
Right Amygdala	1.16 (0.82–1.54)	1.28 (0.99–1.57)	0.65	7.6 (–8.5–48.9)	1.09 (0.44–1.39)	1.25 (0.79–1.55)	0.42	24.2 (–10.2–47.3)
Left NA	0.48 (0.30–0.67)	0.54 (0.42–0.73)	0.64	13.0 (–0.5–38.2)	0.39 (0.17–0.55)	0.52 (0.38–0.82)	0.10	36.3 (–4.1–105.9)
Right NA	0.39 (0.25–0.54)	0.45 (0.37–0.63)	0.47	14.0 (–12–78.2)	0.33 (0.19–0.66)	0.44 (0.28–0.61)	0.36	36.3 (–29.8–86.4)
Brainstem	18.8 (15.4–22.3)	18.5 (14.6–22.1)	0.93	–2.6 (–7.8–8.7)	18.5 (14.1–22.0)	17.5 (14.8–21.0)	0.85	–4.2 (–9.6–5.9)

Volumes are reported as median (range) and percentage differences (%D) are reported as median (estimated 95% confidence intervals). Percentage differences that are significantly different between motion-free and motion-corrupt conventional MPRAGE data are highlighted in bold. GP, globus pallidus; NA, nucleus accumbens.

right caudate nucleus; and poor for the bilateral amygdala and nucleus accumbens (Table 2).

Hippocampal volumes

ICC measures between motion-free conventional MPRAGE data and DISORDER data were excellent for the bilateral CA1, bilateral CA4, bilateral dentate gyrus, bilateral SRLM and bilateral total hippocampal volume; good for the right subiculum, bilateral CA3 and right CA2; and moderate for the left subiculum and left CA2 (Table 3).

ICC measures between motion-corrupt conventional MPRAGE and DISORDER data were excellent for the right CA1; good for the right CA2, right SRLM and right total hippocampus; moderate for the left CA2, right CA3, left CA4 and left total hippocampus; and poor for the bilateral subiculum, left CA1, left CA3, right CA4, bilateral dentate gyrus and left SRLM (Table 3).

Regional brain volumes

ICC measures between motion-free conventional MPRAGE and DISORDER data were excellent for the bilateral WM, right cerebellar cortex, bilateral total cerebellum, anterior, central and posterior CC, lateral ventricles bilateral, third and fourth ventricle; good for the bilateral ventral diencephalon, left cerebellar cortex, mid-anterior and mid-posterior CC; moderate for the left cerebellar WM; and weak for the right cerebellar WM (Supplementary Table 2).

ICC measures between motion-corrupt conventional MPRAGE and DISORDER data were excellent for the left total cerebellum,

posterior CC, bilateral lateral ventricles, third and fourth ventricle; good for the right total cerebellum, left ventral diencephalon, mid-posterior, anterior and mid-anterior CC; moderate for bilateral WM, bilateral cerebellar cortex, right ventral diencephalon and central CC; and poor for bilateral cerebellar WM (Supplementary Table 2).

Cortical metrics

ICC measures between motion-free conventional MPRAGE data and DISORDER data were good or excellent for all cortical measures (Table 4).

ICC measures between motion-corrupt conventional MPRAGE and DISORDER data for cortical metrics were moderate for SA and GM volume bilaterally, and poor for other metrics (bilateral CT, mean curvature, and IGI) (Table 4).

Sensitivity analyses after removing participants with CHD

ICC results after removing participants with CHD are reported in Supplementary Table 3.

Percentage difference between brain morphometric measures

Subcortical grey matter volumes

The median percentage difference for subcortical GM volumes between DISORDER and motion-free conventional MPRAGE data ranged from –1.8 to 14% and for motion-corrupt

TABLE 3 ICC and percentage differences between hippocampal volumes obtained with conventional MPRAGE and DISORDER data.

Region	Motion-free conventional MPRAGE				Motion-corrupt conventional MPRAGE			
	Conventional MPRAGE ($\times 10^3$ mm ³)	DISORDER MPRAGE ($\times 10^3$ mm ³)	ICC	%D	Conventional MPRAGE ($\times 10^3$ mm ³)	DISORDER MPRAGE ($\times 10^3$ mm ³)	ICC	%D
Left subiculum	0.52 (0.48–0.68)	0.51 (0.44–0.68)	0.74	−6.6 (−18.1–7.2)	0.47 (0.19–0.69)	0.47 (0.41–0.66)	0.17	−3.6 (−20.6–95.4)
Right subiculum	0.55 (0.40–0.66)	0.51 (0.39–0.58)	0.81	−6.0 (−19.0–1.6)	0.53 (0.34–0.74)	0.50 (0.38–0.65)	0.31	−2.0 (−31.0–29.2)
Left CA1	0.86 (0.63–1.15)	0.88 (0.68–1.11)	0.99	1.8 (−3.6–6.0)	0.78 (0.49–1.14)	0.83 (0.63–1.06)	0.43	4.0 (−11.7–86.7)
Right CA1	0.93 (0.82–1.15)	0.94 (0.81–1.12)	0.96	0.7 (−3.2–7.1)	0.84 (0.65–1.26)	0.89 (0.70–1.20)	0.91	2.9 (−8.3–13.6)
Left CA2	0.12 (0.08–0.16)	0.11 (0.07–0.13)	0.65	−3.5 (−19.8–28.4)	0.12 (0.04–0.34)	0.11 (0.06–0.21)	0.63	−17.3 (−68.7–41.2)
Right CA2	0.10 (0.07–0.14)	0.094 (0.07–0.12)	0.82	−6.4 (−26.3–19.9)	0.079 (0.04–0.14)	0.094 (0.06–0.12)	0.90	14.0 (−9.7–75.2)
Left CA3	0.32 (0.25–0.40)	0.30 (0.21–0.38)	0.86	−6.9 (−15.9–10.1)	0.32 (0.13–0.55)	0.28 (0.18–0.37)	0.11	−5.8 (−60.3–30.1)
Right CA3	0.25 (0.18–0.33)	0.25 (0.20–0.31)	0.90	−4.3 (−14.0–17.6)	0.21 (0.17–0.29)	0.24 (0.19–0.35)	0.62	10.6 (−8.3–35.3)
Left CA4	0.15 (0.09–0.25)	0.14 (0.09–0.24)	0.94	−5.2 (−25.6–24.8)	0.15 (0.04–0.29)	0.15 (0.08–0.29)	0.57	−3.1 (−34–137.3)
Right CA4	0.19 (0.12–0.31)	0.17 (0.12–0.29)	0.95	−7.0 (−18.5–2.6)	0.20 (0.13–0.31)	0.18 (0.12–0.27)	0.23	−4.7 (−36.2–38.8)
Left DG	0.13 (0.10–0.17)	0.13 (0.10–0.16)	0.95	−2.9 (−12.0–1.4)	0.11 (0.05–0.14)	0.13 (0.10–0.14)	0.38	−0.5 (−8.2–112.4)
Right DG	0.12 (0.10–0.16)	0.13 (0.10–0.16)	0.95	−1.3 (−11.2–6.3)	0.10 (0.07–0.16)	0.13 (0.10–0.15)	0.29	10.1 (−6.0–66.8)
Left SRLM	0.58 (0.50–0.78)	0.57 (0.49–0.70)	0.96	−1.8 (−9.2–2.3)	0.51 (0.24–0.77)	0.55 (0.45–0.66)	0.45	−0.6 (−11.1–103.)
Right SRLM	0.61 (0.51–0.77)	0.59 (0.50–0.73)	0.96	−2.7 (−7.3–3.5)	0.54 (0.43–0.78)	0.57 (0.49–0.76)	0.84	−2.2 (−8.4–23.4)
Left total hippocampus	2.74 (2.30–3.54)	2.65 (2.28–3.20)	0.96	−2.1 (−8.0–0.5)	2.43 (1.32–3.38)	2.52 (2.05–3.17)	0.54	−2.6 (−11.7–21.4)
Right total hippocampus	2.73 (2.35–3.37)	2.66 (2.33–3.18)	0.96	−2.3 (−6.1–0.6)	2.53 (1.94–3.43)	2.60 (2.24–3.44)	0.88	0.3 (−5.9–17.9)

Volumes are reported as median (range) and percentage differences (%D) are reported as median (estimated 95% confidence-intervals). Percentage differences that are significantly different between motion-free and motion-corrupt conventional MPRAGE data are highlighted in bold. CA, cornu ammonius; DG, dentate gyrus; SRLM, stratum radiatum lacunosum and moleculare.

TABLE 4 ICC and percentage differences between cortical measures obtained using conventional MPRAGE and DISORDER data.

Measure	Motion-free conventional MPRAGE				Motion-corrupt conventional MPRAGE			
	Conventional MPRAGE	DISORDER MPRAGE	ICC	%D	Conventional MPRAGE	DISORDER MPRAGE	ICC	%D
Left SA ($\times 10^4$ mm ²)	9.16 (8.08–9.97)	9.67 (8.44–10.68)	0.78	5.0 (0.7–14)	7.97 (6.17–9.88)	9.62 (7.82–12.11)	0.52	22.2 (9.8–33.2)
Right SA ($\times 10^4$ mm ²)	9.12 (7.93–9.97)	9.69 (8.34–10.57)	0.81	5.3 (2.7–12)	8.05 (5.96–9.81)	9.56 (7.88–11.83)	0.53	21.2 (8.6–32.4)
Left GM ($\times 10^5$ mm ³)	2.98 (2.48–3.4)	2.96 (2.45–3.60)	0.98	−0.5 (−4.2–5.7)	2.77 (2.04–3.4)	3.04 (2.39–3.80)	0.73	9.0 (−7.0–29.8)
Right GM ($\times 10^5$ mm ³)	2.97 (2.44–3.4)	2.93 (2.42–3.54)	0.98	−0.2 (−3.9–4.2)	2.70 (1.96–3.4)	3.10 (2.39–3.80)	0.74	11.2 (−3.9–26.4)
Left CT (mm)	2.82 (2.63–2.93)	2.75 (2.51–3.09)	0.78	−1.4 (−6.9–4.7)	2.82 (2.65–3.11)	2.72 (2.45–2.91)	0.26	−4.3 (−17.6–3.9)
Right CT (mm)	2.78 (2.62–2.94)	2.72 (2.50–3.05)	0.81	−1.7 (−5.5–5.0)	2.84 (2.65–3.08)	2.70 (2.45–2.90)	0.09	−5.2 (−15.4–3.7)
Left mean curvature (1/mm)	0.13 (0.12–0.14)	0.13 (0.12–0.14)	0.77	2.4 (−4.6–6.7)	0.15 (0.14–0.16)	0.13 (0.13–0.14)	0.12	−9.1 (−16.2–0.5)
Right mean curvature (1/mm)	0.13 (0.12–0.14)	0.13 (0.12–0.14)	0.76	1.9 (−3.7–7.1)	0.15 (0.14–0.16)	0.13 (0.13–0.14)	0.16	−10.1 (−14.7–2.3)
Left IGI	3.47 (3.26–3.65)	3.48 (3.23–3.68)	0.92	−0.1 (−3.6–3.5)	3.22 (3.08–3.56)	3.47 (3.29–3.95)	0.45	7.6 (0.2–12.7)
Right IGI	3.43 (3.29–3.68)	3.43 (3.26–3.71)	0.92	0.2 (−3.7–4.0)	3.22 (2.97–3.48)	3.45 (3.25–3.89)	0.48	9.1 (0.1–17.2)

Measures are reported as median (range) and percentage differences (%D) are reported as median (estimated 95% confidence-intervals). Percentage differences that are significantly different between motion-free and motion-corrupt conventional MPRAGE data are highlighted in bold. SA, surface area; GM, grey matter volume; CT, cortical thickness; IGI, local gyrification index.

conventional MPRAGE data ranged from −1.4 to 36.3%. Table 2 shows the percentage difference for all subcortical GM volumes. The percentage difference between measures obtained using

DISORDER and motion-corrupt conventional MPRAGE data was significantly greater than those obtained using motion-free conventional MPRAGE data for the bilateral putamen, right

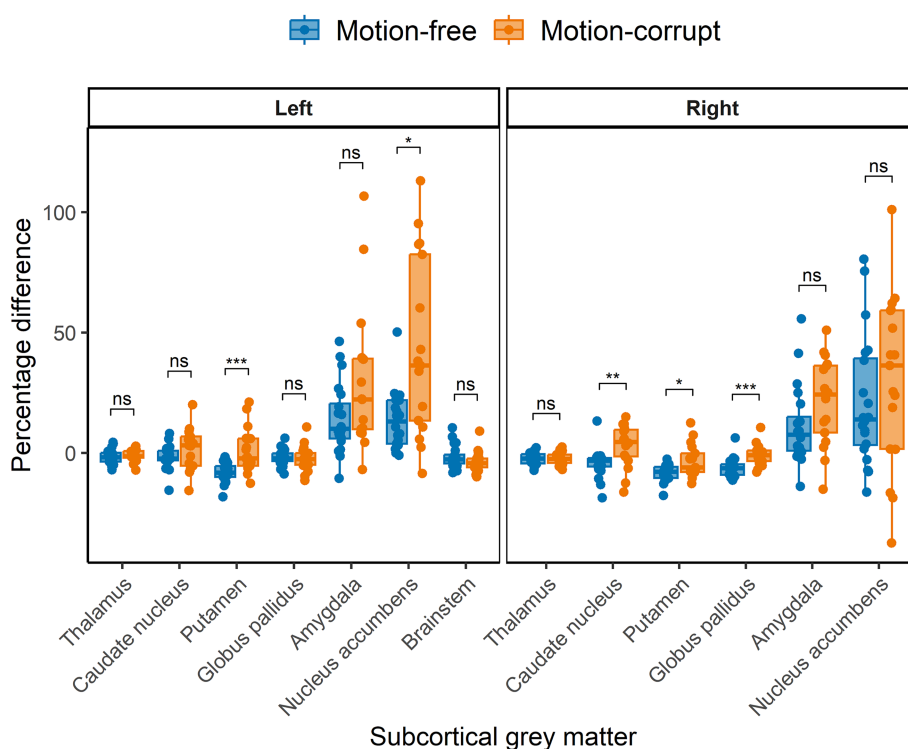


FIGURE 4
Percentage difference ((DISORDER – conventional MPRAGE/conventional MPRAGE) * 100) between subcortical GM volumes obtained using DISORDER vs. motion-free conventional MPRAGE data and DISORDER vs. motion-corrupt conventional MPRAGE data. Results are shown separately for the left and right hemispheres (brainstem is included in the left panel). ns indicates a non-significant difference, * indicates a significant difference at the pFDR < 0.05 level, ** indicates a significant difference at the pFDR < 0.01 level, *** indicates a significant difference at the pFDR < 0.001 level.

caudate nucleus, right globus pallidus and left nucleus accumbens. There was no significant effect of motion on the percentage difference for the volume of any other subcortical GM structure (Figure 4).

Hippocampal volumes

The median percentage difference in hippocampal volumes between DISORDER and motion-free conventional MPRAGE data ranged from -7.0 to 1.8% and for motion-corrupt conventional MPRAGE data ranged from -17.3 to 14% . Table 3 shows the percentage difference for all hippocampal volumes. The percentage difference between hippocampal volumes obtained using DISORDER and motion-corrupt conventional MPRAGE data was significantly greater than those obtained using motion-free conventional MPRAGE data for the right CA2, right CA3, bilateral dentate gyrus and right total hippocampus. There was no significant effect of motion on the percentage difference for the volume of any other hippocampal measure (Figure 5).

Regional brain volumes

The median percentage difference in regional brain volumes between DISORDER and motion-free conventional MPRAGE data ranged from -6.3 to 7.4% and for motion-corrupt conventional MPRAGE data ranged from -8.7 to 13% . Supplementary Table 2 shows the percentage difference for all regional brain volumes. The percentage difference between measures obtained using DISORDER and motion-corrupt conventional MPRAGE data was significantly greater than those

obtained using motion-free conventional MPRAGE data for the bilateral WM, left total cerebellum and mid-anterior corpus callosum volumes. There was no significant effect of motion on the percentage difference for any other regional brain volume (Supplementary Figure 2).

Cortical metrics

The median percentage difference of regional brain volumes between DISORDER and motion-free conventional MPRAGE data ranged from -0.5 to 5.3% and for motion-corrupt conventional MPRAGE data ranged from -10.1 to 22.2% . Table 4 shows the percentage difference for all cortical metrics. The percentage difference between measures obtained using DISORDER and motion-corrupt conventional MPRAGE data was significantly greater than those obtained using motion-free conventional MPRAGE data for the bilateral SA, cortical GM volume, mean curvature and IGI. There was no significant effect of motion on the percentage difference for CT bilaterally (Figure 6).

Sensitivity analyses after removing participants with CHD

The test gave the same results when the participants with CHD were removed from the analyses (Supplementary Table 3).

Hemispheric differences in brain morphometric measures

Percentage differences between the left and right hemispheres were not significant when comparing DISORDER and motion-free

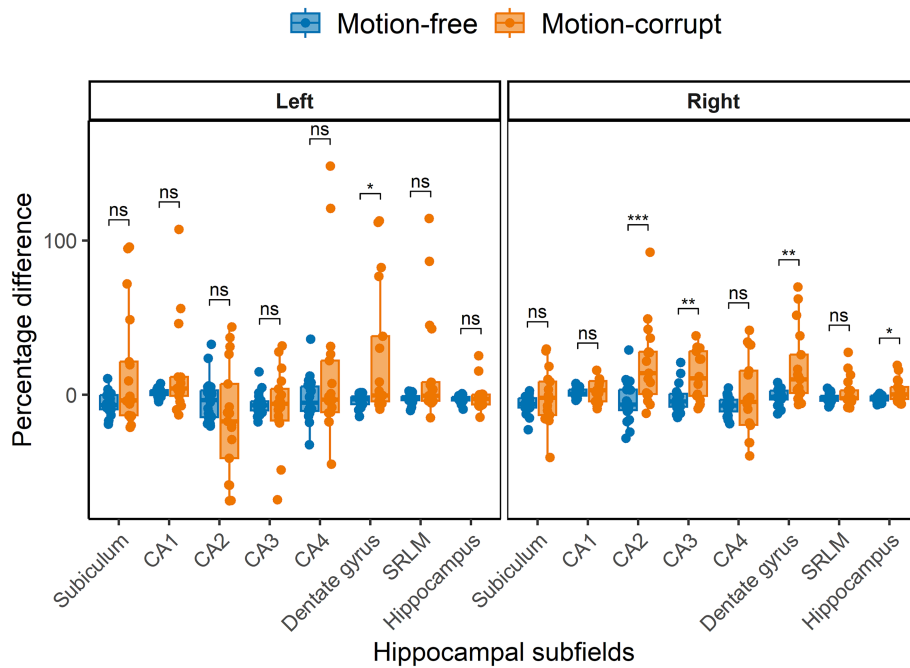


FIGURE 5

Percentage difference between hippocampal volumes obtained using DISORDER vs. motion-free conventional MPRAGE data and DISORDER vs. motion-corrupt conventional MPRAGE data. Results are shown separately for the left and right hemispheres. CA, cornu ammonis; SRLM, stratum radiatum lacunosum and moleculare. ns indicates a non-significant difference, * indicates a significant difference at the pFDR < 0.05 level, ** indicates a significant difference at the pFDR < 0.01 level, *** indicates a significant difference at the pFDR < 0.001 level.

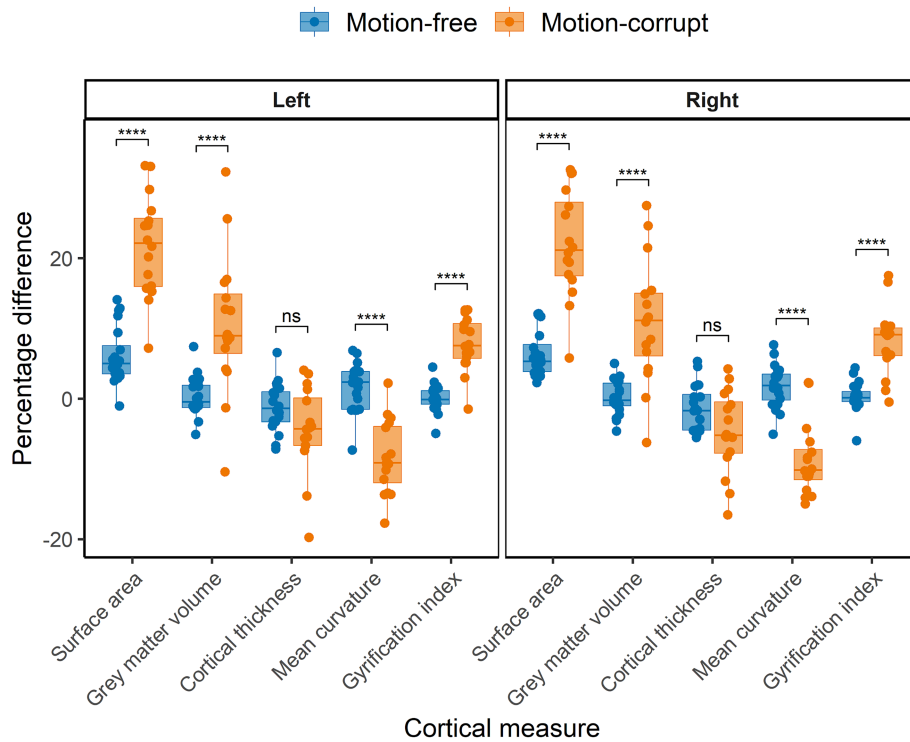


FIGURE 6

Percentage difference between cortical measures obtained using DISORDER vs. motion-free conventional MPRAGE data and DISORDER vs. motion-corrupt conventional MPRAGE data. Results are shown separately for the left and right hemispheres. ns indicates a non-significant difference, **** indicates a significant difference at the pFDR < 0.0001 level.

conventional MPRAGE data. However, significant inter-hemispheric differences were identified between DISORDER and motion-corrupt conventional MPRAGE data for 5 of 25 structures assessed (caudate nucleus, CA2, CA3, cortical GM and cerebellar WM volumes). Percentage differences between the left and right hemispheres are reported in [Supplementary Tables 4–7](#) and shown in [Supplementary Figures 3–6](#).

Discussion

In this study, we evaluated the use of the DISORDER scheme for pediatric brain morphometry by comparing regional and subcortical GM brain volumes, hippocampal subfield volumes and cortical measures derived from conventional linear phase encoding MPRAGE images with those of MPRAGE acquired with the DISORDER sampling scheme in children aged between 7 and 8 years. We studied a wide range of brain structures to include regions that would be of interest to a wide range of pediatric neuroimaging studies. Our results suggest that, for most regions, brain morphometric measures obtained from DISORDER MPRAGE and motion-free conventional MPRAGE data are highly consistent. Brain morphometric measures obtained from motion-corrupt conventional MPRAGE and DISORDER data showed greater variance in concordance, particularly in hippocampal and cortical metrics.

Obtaining high-quality MR images in children is challenging, and head motion is a major cause of image degradation in pediatric neuroimaging. Previous work demonstrated that the DISORDER framework improved image quality in a pediatric cohort (age range 2–18 years) ([Vecchiato et al., 2021](#)). In our study, a high proportion of data acquired with the conventional acquisition had evidence of motion artifact (17 out of 37 children, 46%), highlighting the need for motion correction approaches in pediatric populations. Furthermore, in 14/17 (82%) children with motion-corrupt conventional MPRAGE data, image quality was good following a motion corrected DISORDER acquisition, and only minimal motion artefact was apparent in the remaining 3 datasets. These findings suggest that DISORDER may reduce the number of failed examinations in clinical settings, in addition to being a useful tool in research neuroimaging studies.

Our results show that cortical measures obtained using DISORDER and motion-free conventional MPRAGE acquisitions were highly consistent. However, we found that cortical measures showed poorer concordance between DISORDER and motion-corrupt conventional MPRAGE data. We also report a significant effect of motion, as assessed by the percentage difference between measures obtained using DISORDER and motion-free and motion-corrupt conventional MPRAGE data, on most cortical measures, with >20% difference in SA between DISORDER and motion-corrupt conventional MPRAGE data (compared to a percentage difference of 5% between DISORDER and motion-free conventional MPRAGE data in SA measures), highlighting the importance of correcting for head motion when obtaining cortical morphometric measures. Our findings are consistent with previous studies that demonstrated a reduction in estimates of cortical GM volume ([Reuter et al., 2015](#); [Alexander-Bloch et al., 2016](#)) and an increase in estimates of mean curvature ([Alexander-Bloch et al., 2016](#)) with subject motion.

In addition to cortical measures, we found that most subcortical GM and regional brain volumes showed excellent or good agreement

between motion-free conventional and DISORDER acquisitions and the percentage difference in subcortical GM and regional volumes obtained from motion-free conventional MPRAGE were similar to percentage differences reported in scan-rescan reliability studies in adults ([Morey et al., 2010](#)). Interestingly, we found good-excellent agreement for 8 out of 13 subcortical GM and 11 out of 19 regional brain volumes between motion-corrupt conventional MPRAGE and DISORDER data. Over 60% of subcortical GM and 79% of regional brain volumes showed no significant effect of motion when comparing the percentage difference in volumes obtained from motion-free and motion-corrupt conventional MPRAGE to DISORDER data. Our findings are supported by previous work ([Kemenczky et al., 2022](#)) which reported good-excellent dice spatial overlap and low absolute volumetric differences between subcortical segmentations acquired with and without motion artifacts, suggesting that segmentation of these structures may have a lower sensitivity to motion compared to cortical regions.

It is notable that agreement between DISORDER and conventional MPRAGE data for amygdala and nucleus accumbens volumes were poor-moderate for both motion-free and motion-corrupt data. Less reliable segmentations of the amygdala and nucleus accumbens have been demonstrated in pediatric test-retest studies ([Kecskemeti and Alexander, 2020](#)) and in studies comparing automated segmentation to manual delineation ([Lidauer et al., 2022](#)), suggesting that the segmentation of these structures may be more susceptible to measurement error due to their small size ([Morey et al., 2010](#)). The amygdala and nucleus accumbens also demonstrated large percentage volume differences (>20 and 36% respectively) between DISORDER and motion-corrupt conventional MPRAGE data. Of note, the percentage volume differences observed here between DISORDER and motion-free conventional MPRAGE data for the amygdala and nucleus accumbens (7–14%) are similar to those reported in a scan-rescan study in adults using FSL-FIRST ([Morey et al., 2010](#)). The large differences in estimates of brain morphometry in motion-corrupt MRI data have consequences for pediatric neuroimaging research, particularly case-control studies where reported morphometric differences may be related to motion-related bias and not genuine biological differences between groups.

Several studies have highlighted altered hippocampal volumetry in pediatric clinical populations, including in children with epilepsy ([Peng et al., 2022](#)), CHD ([Fontes et al., 2019](#)), and ADHD ([Al-Amin et al., 2018](#)). However, in addition to the amygdala and nucleus accumbens, the hippocampus can be challenging to segment due to the interindividual variability in hippocampal size and anatomy ([Lynch et al., 2019](#)). In this study, we showed that volumes of hippocampal subfields were similar between motion-free conventional MPRAGE and DISORDER data. However, hippocampal volumes showed more variability between acquisitions for motion-corrupt MPRAGE data. Furthermore, the percentage difference between DISORDER and motion-corrupt volumes of some hippocampal structures was >10%. Our data highlight that good quality MR data is required for hippocampal subfield segmentation in order to assess differences in these structures between at risk groups and controls, and to investigate associations with neurodevelopmental outcomes.

It is important to note that cerebellar WM demonstrated weak to moderate agreement between both motion-free and motion-corrupt conventional MPRAGE and DISORDER data. Previous work assessing test–retest agreement of automated tools for cerebellar segmentation in adults reported lower ICC values and greater volume differences in FreeSurfer-derived cerebellar WM volumes compared to cerebellar GM volumes (Sörös et al., 2021), highlighting that care should be taken when interpreting results in these regions. However, in our study, the total cerebellar (cerebellar GM + cerebellar WM) volume demonstrated good–excellent agreement between DISORDER and conventional MPRAGE data, suggesting that studies focusing on the whole cerebellum can reliably use measures derived from DISORDER data.

Our results show that percentage differences between the left and right hemispheres were not significant when comparing measures obtained from DISORDER and motion-free conventional MPRAGE data. However, we found significant inter-hemispheric differences between DISORDER and motion-corrupt conventional MPRAGE data for 5 of 25 structures assessed. These findings suggest that motion artifacts may bias the assessment of hemispheric differences in brain morphometric measures, highlighting the importance of correcting for head motion in studies that assess structural brain asymmetry.

There were no changes in the effect of motion when assessing percentage differences between morphometric measures when the individuals with CHD were removed from the analyses. ICC classes of agreement between morphometric measures obtained using motion-corrupt MPRAGE and DISORDER data changed for almost one-quarter of regions assessed after removing the CHD participants. However, when comparing motion-free conventional MPRAGE and DISORDER data, only one region changed agreement classification after removing children with CHD from the analyses (left total cerebellar volume, from excellent to good, ICC 0.91 to 0.90), suggesting our findings comparing DISORDER and good quality MPRAGE data are not biased by the inclusion of children with CHD in our sample.

Limitations and future directions

We studied a narrow age range, between 7 and 8 years. In addition, our sample size was limited. Future studies incorporating a wider age range and with larger samples could further validate the use of DISORDER for brain morphometric analyses. Additionally, future studies with a larger sample size would benefit from training machine-learning based methods with pediatric DISORDER data for automatic motion artifact detection.

The conventional MPRAGE acquisition was acquired with an acceleration factor of 2, while the DISORDER MPRAGE acquisition was acquired without acceleration. Our rationale for this approach was that under-sampled image acquisitions have more widely spaced k-space samples and we have found that the most robust strategy for motion corrected DISORDER scans is to have reduced acceleration. Limiting acceleration makes scans longer, which could increase the risk of motion, but improves performance in correction. For non-motion corrected acquisitions, there is likely to be a benefit in shortening acquisition time to minimize risk of severe motion during

data collection. Our aim was to compare effective strategies of each type of approach rather than to match acquisition durations. Furthermore, matching SNR using a longer conventional scan (with no motion correction) would have increased the likely damage from motion, and so worsened performance. Given limitations in total examination length that the subjects could be expected to tolerate, it was not feasible to add the linking scans of shorter DISORDER and longer conventional scans, but we hope that the binary comparison we provided was a good choice to help provide evidence by comparing between choices future researchers might make in practice.

This work is part of an on-going study that aims to assess the neuroimaging correlates of neurodevelopment in children with CHD and heart-healthy children from a community sample (ICONIC study). Future studies could use DISORDER for brain morphometric analysis to explore group differences between children with CHD and other at-risk groups and typically developing children.

Conclusion

DISORDER enables quantitative structural MRI in difficult-to-image pediatric populations and will facilitate quantitative morphometry in research studies. Our results suggest that morphometric measures obtained using DISORDER retrospective motion correction are largely concordant with those obtained using motion-free conventional MPRAGE data. Motion corrected DISORDER improves the overall accuracy of most cortical morphometric measures and some subcortical volumes when compared to motion-corrupt conventional MPRAGE data. This study validates the use of DISORDER for brain morphometric studies in children.

Data availability statement

The raw data supporting the conclusions of this article will be made available by the authors, without undue reservation.

Ethics statement

The studies involving humans were approved by Wales Research Ethics Committee. The studies were conducted in accordance with the local legislation and institutional requirements. Written informed consent for participation in this study was provided by the participants' legal guardians/next of kin.

Author contributions

BG-E: Data curation, Formal analysis, Investigation, Methodology, Writing – original draft, Visualization. YB: Methodology, Writing – review & editing, Software. AB: Writing – review & editing, Supervision, Data curation. CC: Writing – review & editing, Methodology. AP: Writing – review & editing, Methodology. SA: Methodology, Writing – review & editing. AC: Data curation, Writing – review & editing. CN:

Supervision, Writing – review & editing. MC: Data curation, Writing – review & editing. PC: Writing – review & editing, Data curation. AE: Methodology, Writing – review & editing. MR: Methodology, Writing – review & editing. JO'M: Methodology, Supervision, Writing – review & editing. RT-T: Methodology, Writing – review & editing. SM: Methodology, Writing – review & editing. LC-G: Methodology, Writing – review & editing, Software. JH: Methodology, Writing – review & editing. SC: Conceptualization, Data curation, Formal analysis, Funding acquisition, Investigation, Methodology, Project administration, Resources, Supervision, Validation, Writing – review & editing.

Funding

The author(s) declare that financial support was received for the research and/or publication of this article. This research was funded by the Medical Research Council UK (MR/V002465/1). This work was supported by core funding from the Wellcome/ EPSRC Centre for Medical Engineering [WT203148/Z/16/Z] and by the National Institute for Health and Care Research (NIHR) Clinical Research Facility at Guy's and St Thomas' NHS Foundation Trust. The views expressed are those of the author(s) and not necessarily those of the NHS, the NIHR, or the Department of Health and Social Care.

Acknowledgments

We would like to thank the families who participated in this study.

References

- Ai, L., Craddock, R. C., Tottenham, N., Dyke, J. P., Lim, R., Colcombe, S., et al. (2021). Is it time to switch your T1W sequence? Assessing the impact of prospective motion correction on the reliability and quality of structural imaging. *NeuroImage* 226:117585. doi: 10.1016/j.neuroimage.2020.117585
- Al-Amin, M., Zinchenko, A., and Geyer, T. (2018). Hippocampal subfield volume changes in subtypes of attention deficit hyperactivity disorder. *Brain Res.* 1685, 1–8. doi: 10.1016/j.brainres.2018.02.007
- Alexander-Bloch, A., Clasen, L., Stockman, M., Ronan, L., Lalonde, F., Giedd, J., et al. (2016). Subtle in-scanner motion biases automated measurement of brain anatomy from in vivo MRI: motion Bias in analyses of structural MRI. *Hum. Brain Mapp.* 37, 2385–2397. doi: 10.1002/hbm.23180
- Bautista, T., O'Muircheartaigh, J., Hajnal, J., and Tournier, J-D. Removal of Gibbs ringing artefacts for 3D acquisitions using subvoxel shifts. In: Proceedings of the 30th annual meeting of ISMRM, online. (2021).
- Benjamini, Y., and Hochberg, Y. (1995). Controlling the false discovery rate: a practical and powerful approach to multiple testing. *J. R. Stat. Soc. Ser. B Stat Methodol.* 57, 289–300. doi: 10.1111/j.2517-6161.1995.tb02031.x
- Biffen, S. C., Warton, C. M. R., Dodge, N. C., Molteno, C. D., Jacobson, J. L., Jacobson, S. W., et al. (2020). Validity of automated FreeSurfer segmentation compared to manual tracing in detecting prenatal alcohol exposure-related subcortical and corpus callosal alterations in 9- to 11-year-old children. *NeuroImage Clin.* 28:102368. doi: 10.1016/j.nicl.2020.102368
- Cordero-Grande, L., Ferrazzi, G., Teixeira, R. P. A. G., O'Muircheartaigh, J., Price, A. N., and Hajnal, J. V. (2020). Motion-corrected MRI with DISORDER: distributed and incoherent sample orders for reconstruction deblurring using encoding redundancy. *Magn. Reson. Med.* 84, 713–726. doi: 10.1002/mrm.28157
- Cordero-Grande, L., Teixeira, R. P. A. G., Hughes, E. J., Hutter, J., Price, A. N., and Hajnal, J. V. (2016). Sensitivity encoding for aligned multishot magnetic resonance reconstruction. *IEEE Trans Comput Imaging.* 2, 266–280. doi: 10.1109/TCL.2016.2557069
- Dale, A. M., Fischl, B., and Sereno, M. I. (1999). Cortical surface-based analysis I: segmentation and surface reconstruction. *NeuroImage* 9, 179–194. doi: 10.1006/nimg.1998.0395
- DeKraker, J., Haast, R. A., Yousif, M. D., Karat, B., Lau, J. C., Köhler, S., et al. (2022). Automated hippocampal unfolding for morphometry and subfield segmentation with HippUnfold. *eLife* 11:e77945. doi: 10.7554/eLife.77945
- Desikan, R. S., Ségonne, F., Fischl, B., Quinn, B. T., Dickerson, B. C., Blacker, D., et al. (2006). An automated labeling system for subdividing the human cerebral cortex on MRI scans into gyral based regions of interest. *NeuroImage* 31, 968–980. doi: 10.1016/j.neuroimage.2006.01.021
- Fischl, B., Salat, D. H., Busa, E., Albert, M., Dieterich, M., Haselgrove, C., et al. (2002). Whole brain segmentation. *Neuron* 33, 341–355. doi: 10.1016/S0896-6273(02)00569-X
- Fischl, B., Sereno, M. I., and Dale, A. M. (1999). Cortical surface-based analysis II: inflation, flattening, and a surface-based coordinate system. *NeuroImage* 9, 195–207. doi: 10.1006/nimg.1998.0396
- Fontes, K., Rohlicek, C. V., Saint-Martin, C., Gilbert, G., Easson, K., Majnemer, A., et al. (2019). Hippocampal alterations and functional correlates in adolescents and young adults with congenital heart disease. *Hum. Brain Mapp.* 40, 3548–3560. doi: 10.1002/hbm.24615
- Gilmore, A. D., Buser, N. J., and Hanson, J. L. (2021). Variations in structural MRI quality significantly impact commonly used measures of brain anatomy. *Brain Inform.* 8:7. doi: 10.1186/s40708-021-00128-2
- Glasser, M. F., Sotiropoulos, S. N., Wilson, J. A., Coalson, T. S., Fischl, B., Andersson, J. L., et al. (2013). The minimal preprocessing pipelines for the human connectome project. *NeuroImage* 80, 105–124. doi: 10.1016/j.neuroimage.2013.04.127
- Hoopes, A., Mora, J. S., Dalca, A. V., Fischl, B., and Hoffmann, M. (2022). SynthStrip: skull-stripping for any brain image. *NeuroImage* 260:119474. doi: 10.1016/j.neuroimage.2022.119474
- Kecksemeti, S. R., and Alexander, A. L. (2020). Test-retest of automated segmentation with different motion correction strategies: a comparison of prospective versus retrospective methods. *NeuroImage* 209:116494. doi: 10.1016/j.neuroimage.2019.116494
- Kellner, E., Dhital, B., Kiselev, V. G., and Reiser, M. (2016). Gibbs-ringing artifact removal based on local subvoxel-shifts. *Magn. Reson. Med.* 76, 1574–1581. doi: 10.1002/mrm.26054

Conflict of interest

RT-T was employed by MR Research Collaborations, Siemens Healthcare Limited.

The remaining authors declare that the research was conducted in the absence of any commercial or financial relationships that could be construed as a potential conflict of interest.

Generative AI statement

The authors declare that no Gen AI was used in the creation of this manuscript.

Publisher's note

All claims expressed in this article are solely those of the authors and do not necessarily represent those of their affiliated organizations, or those of the publisher, the editors and the reviewers. Any product that may be evaluated in this article, or claim that may be made by its manufacturer, is not guaranteed or endorsed by the publisher.

Supplementary material

The Supplementary material for this article can be found online at: <https://www.frontiersin.org/articles/10.3389/fnins.2025.1534924/full#supplementary-material>

- Kemenczky, P., Vakli, P., Somogyi, E., Homolya, I., Hermann, P., Gál, V., et al. (2022). Effect of head motion-induced artefacts on the reliability of deep learning-based whole-brain segmentation. *Sci. Rep.* 12:1618. doi: 10.1038/s41598-022-05583-3
- Koo, T. K., and Li, M. Y. (2016). A guideline of selecting and reporting Intraclass correlation coefficients for reliability research. *J. Chiropr. Med.* 15, 155–163. doi: 10.1016/j.jcm.2016.02.012
- Lidauer, K., Pulli, E. P., Copeland, A., Silver, E., Kumpulainen, V., Hashempour, N., et al. (2022). Subcortical and hippocampal brain segmentation in 5-year-old children: validation of FSL-FIRST and FreeSurfer against manual segmentation. *Eur. J. Neurosci.* 56, 4619–4641. doi: 10.1111/ejn.15761
- Lynch, K. M., Shi, Y., Toga, A. W., and Clark, K. A. (2019). Hippocampal shape maturation in childhood and adolescence. *Cereb. Cortex* 29, 3651–3665. doi: 10.1093/cercor/bhy244
- Maclaren, J., Herbst, M., Speck, O., and Zaitsev, M. (2013). Prospective motion correction in brain imaging: a review. *Magn. Reson. Med.* 69, 621–636. doi: 10.1002/mrm.24314
- Mayer, K. N., Latal, B., Knirsch, W., Scheer, I., von Rhein, M., Reich, B., et al. (2016). Comparison of automated brain volumetry methods with stereology in children aged 2 to 3 years. *Neuroradiology* 58, 901–910. doi: 10.1007/s00234-016-1714-x
- Morey, R. A., Selgrade, E. S., Wagner, H. R., Huettel, S. A., Wang, L., and McCarthy, G. (2010). Scan-rescan reliability of subcortical brain volumes derived from automated segmentation. *Hum. Brain Mapp.* 31, 1751–1762. doi: 10.1002/hbm.20973
- Patenaude, B., Smith, S. M., Kennedy, D. N., and Jenkinson, M. (2011). A Bayesian model of shape and appearance for subcortical brain segmentation. *NeuroImage* 56, 907–922. doi: 10.1016/j.neuroimage.2011.02.046
- Peng, S.-J., Hsieh, K. L.-C., Lin, Y.-K., Tsai, M.-L., Wong, T.-T., and Chang, H. (2022). Febrile seizures reduce hippocampal subfield volumes but not cortical thickness in children with focal onset seizures. *Epilepsy Res.* 179:106848. doi: 10.1016/j.eplepsyres.2021.106848
- Pulli, E. P., Silver, E., Kumpulainen, V., Copeland, A., Merisaari, H., Saunavaara, J., et al. (2022). Feasibility of FreeSurfer processing for T1-weighted brain images of 5-year-olds: Semiautomated protocol of FinnBrain neuroimaging lab. *Front. Neurosci.* 16:874062. doi: 10.3389/fnins.2022.874062
- Reuter, M., Tisdall, M. D., Qureshi, A., Buckner, R. L., van der Kouwe, A. J. W., and Fischl, B. (2015). Head motion during MRI acquisition reduces gray matter volume and thickness estimates. *NeuroImage* 107, 107–115. doi: 10.1016/j.neuroimage.2014.12.006
- Ripart, M., DeKraker, J., Eriksson, M. H., Piper, R. J., Gopinath, S., Parasuram, H., et al. (2023). Automated and interpretable detection of hippocampal sclerosis in temporal lobe epilepsy: AID-HS. *medRxiv*. doi: 10.1101/2023.10.13.23296991
- Sandman, C. A., Head, K., Muftuler, L. T., Su, L., Buss, C., and Davis, E. P. (2014). Shape of the basal ganglia in preadolescent children is associated with cognitive performance. *NeuroImage* 99, 93–102. doi: 10.1016/j.neuroimage.2014.05.020
- Schaer, M., Cuadra, M. B., Schmansky, N., Fischl, B., Thiran, J.-P., and Eliez, S. (2012). How to measure cortical folding from MR images: a step-by-step tutorial to compute local Gyrification index. *J. Vis. Exp.* 59:e3417. doi: 10.3791/3417
- Schaer, M., Cuadra, M. B., Tamarit, L., Lazeyras, F., Eliez, S., and Thiran, J.-P. (2008). A surface-based approach to quantify local cortical Gyrification. *IEEE Trans. Med. Imaging* 27, 161–170. doi: 10.1109/TMI.2007.903576
- Schoemaker, D., Buss, C., Head, K., Sandman, C. A., Davis, E. P., Chakravarty, M. M., et al. (2016). Hippocampus and amygdala volumes from magnetic resonance images in children: assessing accuracy of FreeSurfer and FSL against manual segmentation. *NeuroImage* 129, 1–14. doi: 10.1016/j.neuroimage.2016.01.038
- Sörös, P., Wölk, L., Bantel, C., Bräuer, A., Klawonn, F., and Witt, K. (2021). Replicability, repeatability, and long-term reproducibility of cerebellar morphometry. *Cerebellum* 20, 439–453. doi: 10.1007/s12311-020-01227-2
- Thompson-Lake, D. G. Y., Scerri, T. S., Block, S., Turner, S. J., Reilly, S., Kefalianos, E., et al. (2022). Atypical development of Broca's area in a large family with inherited stuttering. *Brain* 145, 1177–1188. doi: 10.1093/brain/awab364
- Tustison, N. J., Avants, B. B., Cook, P. A., Yuanjie Zheng, Egan, A., Yushkevich, P. A., et al. (2010). N4ITK: improved N3 Bias correction. *IEEE Trans. Med. Imaging* 29, 1310–1320. doi: 10.1109/TMI.2010.2046908
- Vecchiato, K., Egloff, A., Carney, O., Siddiqui, A., Hughes, E., Dillon, L., et al. (2021). Evaluation of DISORDER: retrospective image motion correction for volumetric brain MRI in a pediatric setting. *Am. J. Neuroradiol.* 42, 774–781. doi: 10.3174/AJNR.A7001